Korean J. Chem. Eng., 33(1), 63-72 (2016)
DOI: 10.1007/s11814-015-0056-4

pISSN: 0256-1115
eISSN: 1975-7220

Modeling and experimental studies of ammonia absorption in a spray tower

Jie Zhu, Zhenhua Liu, Jie Bai, Yunfeng Yang, Qin Peng, Shichao Ye†, and Mingzhe Chen

School of Chemical Engineering, Sichuan University, Chengdu 610065, China
(*Received 18 December 2014 • accepted 22 March 2015*)

Abstract−We did an experimental study on ammonia absorption in a spray tower. The kinetic characteristics of droplets were investigated by considering the forces acting on a droplet. The gas-phase mass transfer coefficient was deduced with the Colburn analogy method. A simplified model for predicting NH_3 capture with a spray tower has been presented based on mass transfer and ionic equilibrium, which was successfully validated against experimental data. The influences and the sensitivity analysis of main operating parameters on the absorption efficiency were analyzed. As the most sensitive parameter, the mean droplet diameter was obtained by fitting experimental data with an empirical correlation. The distributions of two typical process parameters along the absorber were also simulated. Decreasing the pH value of absorbent is an effective but restrictive way to strengthen the mass transfer rate on account of insufficient liquid-side resistance.

Keywords: Spray Tower, Ammonia, Model, Mass Transfer Coefficient, Absorption Efficiency

INTRODUCTION

A colorless, toxic, pungent gas, NH_3, is extensively used for manufacturing fertilizers and a wide variety of nitrogen-containing organic and inorganic chemicals [1,2]. Ammonia emission from various branches of industry and livestock agriculture has become one of the major environmental concerns [3,4]. In particular, the emission of nitro-phosphate tail gas with large discharge, high moisture content and low NH_3 concentration has led to severe resource waste and environmental pollution.

Up to now, various processes have been available for treating the NH_3-laden gas, including catalytic oxidation, biological filtration, liquid absorption and solid adsorption [2,5-8]. A potential method for gas purification, without secondary pollution, is to disperse some acid solution (such as dilute nitric acid) to recycle NH_3 for producing fertilizers, counting on the acid-base neutralization reactions. Besides, as a kind of absorbent, the dilute nitric acid is abundant in a nitrogen fertilizer plant. The liquid absorption with packed tower seems to be an efficient approach for NH_3 removal because of higher specific surface area and lower operating cost [9]. However, packed towers suffer from various operational problems, such as, blocking, scaling, and channeling [10]. In addition, to handle the large amount of tail gas with low NH_3 concentration from a fertilizer plant requires a very large absorber, resulting in expensive construction and maintenance. By contrast, spray towers have been widely researched for the well-known superiorities, including simple construction, lack of complicated spray elements, resistance to corrosion, large handling capacity and low investment costs [11].

Over the past few decades, considerable numbers of studies have been conducted on mass transfer performance in spray towers. However, the majority of these were committed to flue gas desulfurization [12-15], and rarely encountered any gas purification fields involving NH_3. Ocfemia et al. set up a spray system to reduce NH_3 emission from livestock buildings, with low inlet NH_3 concentration and high airflow rate, and the NH_3 removal efficiency as affected by airflow rate and nozzle settings was obtained [16]. Javed et al. investigated the enhancement of mass transfer in a laboratory-scale spray tower using swirling gas flow with the experimental system of air-NH_3/water. The results indicated that the volumetric mass transfer coefficient was highly influenced by the gas-liquid flow pattern [17]. However, the studies are only applicable under some dedicated conditions; so far, there is a lack of specialized research on NH_3 abatement from industrial tail gas with spray absorber. Additionally, for a general spray tower, the droplets are generated by pressure nozzle; thus the prediction of mass transfer area seems to be difficult owning to numerous factors: gas and liquid velocities, coalescence phenomena, drop oscillation and dispersion, and wall effect [18,19].

In fact, as the basic unit of droplets swarm scavenging in spray tower, the NH_3 absorption behavior of a moving droplet, with diameter ranging from tens to hundreds of microns, has been investigated numerically in detail. Adamowicz et al. investigated the simultaneous absorption of SO_2 and NH_3 by raindrops, and ignored the liquid-phase mass transfer resistance for the case of rapid convection in the drop [20]. However, Taniguchi et al. proved that the NH_3 uptake by water droplet involves both gas- and liquid-phase mass transfer resistances [21]. Adewuyi et al. proposed a physical-chemical model to investigate NH_3 absorption by water drops from trace gas mixtures, and the results demonstrated that the absorption behavior of droplets was strongly dependent on droplet diameter and drop distance [22]. Unfortunately, average droplet diameter in industrial scale spray tower is about 1-3 mm, and only a few physical factors on absorption rate of millimeter-size droplet were performed

†To whom correspondence should be addressed.
E-mail: shichaoye@sina.com

by Eremin et al. with the condition of high NH_3 concentration in gas phase [3]. Besides, the evolution of both physical and chemical properties of droplets during the falling process is still insufficient.

The purpose of this paper is to investigate the performance characteristics of a spray tower for NH_3 capture in terms of absorption efficiency, and develop a mathematical model for describing the NH_3 absorption system. A novel lab-pilot spray absorber was designed for eliminating the disturbances of uncertain factors to the mass transfer area as much as possible. Detailed acid-base property inside droplets at different initial pH values will be addressed. Insights are also given on the contribution of pH value on the fraction of gas-phase mass transfer resistance along the absorber based on the model simulations.

EXPERIMENTAL SECTION

The experimental apparatus, shown in Fig. 1, mainly consists of a pretreatment system, an absorption tower and a liquid reservoir. The simulated mixture with NH_3 concentration in the range of 800-6,000 mg/m^3 was generated by assembling air and NH_3 into a mixer. The raw gas entered the tower at the bottom and came out from the top. The clean gas left the system after the entrained droplets were removed by a cyclone separator. The dilute nitric acid from the liquid reservoir was sprayed at the top over a multihole distributor (perforated plate) with a dedicated pump, and the experiments were carried out without liquid recirculation. The droplets fell down and flowed out from the bottom after reacting with the NH_3-containing gas. In this way, the flowing gas stream contacted with the droplet swarm in a counter-current flow arrangement. The pH value of absorbent was adjusted with dilute nitric acid, and measured by a calibrated pH meter. The concentration of NH_3 in the gas mixture was measured both at the gas inlet and outlet, using a spectrophotometric method with Nessler reagent. The absorbent flow rate was indicated by a calibrated rotameter and controlled by a specialized valve.

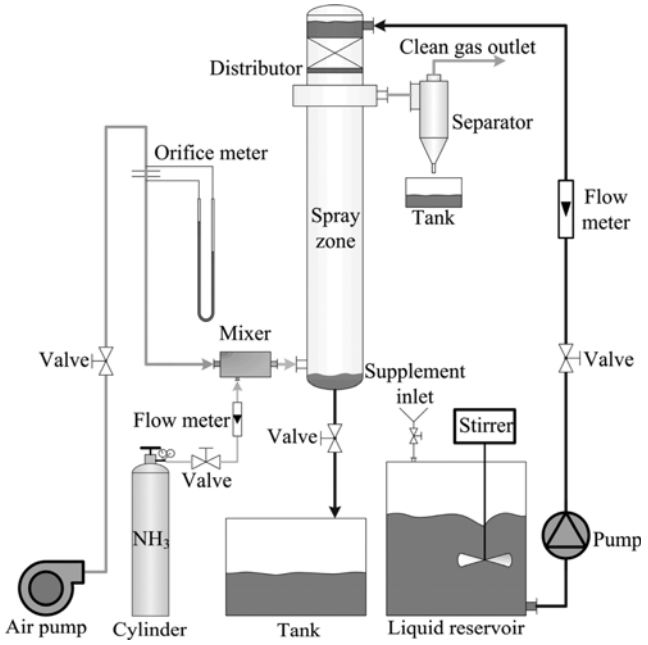

Fig. 1. Schematic diagram of ammonia absorption system.

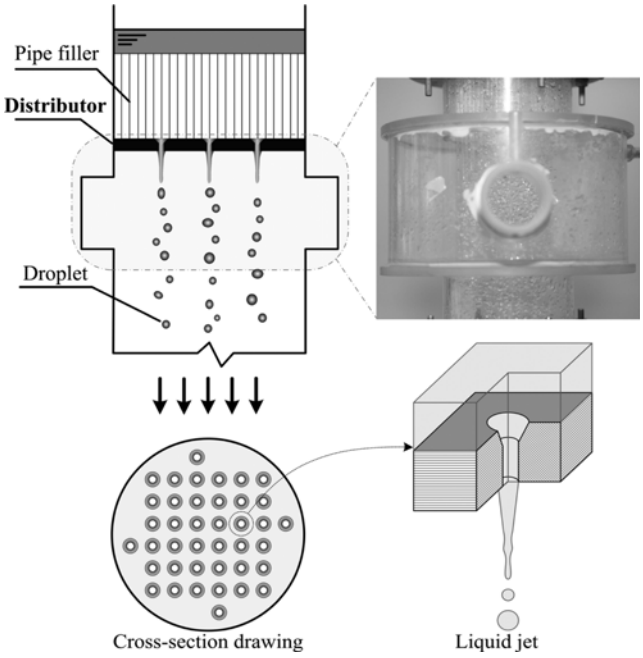

Fig. 2. Mechanism of distributor.

The spray zone is a vertical cylindrical Perspex pipe with measurements of 1.77 m high and 0.1 m inside diameter. At the top of the zone, a multihole distributor is provided for generating droplets (as shown in Fig. 2), and 40 holes with 1.5 mm diameter are dispersed uniformly in the form of orthogonal distribution. The absorbent formed liquid jet firstly, then broke into droplets gradually due to the gravity and surface tension [23]. As compared to a pressure nozzle, droplets formed by the perforated plate were able to drop vertically, because the jet Reynolds numbers were relatively low at our experimental conditions, and the formed droplets were almost without horizontal velocity according to Rayleigh breakup mechanism [24]. Therefore, both coalescence and the wall effect were largely eliminated. The pipe filler consisting of thin tubes was used to eliminate the turbulent flow over the perforated plate. Details of the operating conditions are shown in Table 1.

The drop size in spray tower was measured with photographic technique. At different experimental conditions, photographs of the droplet swarm were obtained with a digital single lens reflex (Canon EOS 5D Mark II). The shutter speed was set as 1/8000 sec-

Table 1. Experimental conditions of the spray tower

Parameter	Unit	Condition
β	m^3/m^2·h	25-78
u_g	m/s	1.2-2.7
c_{NH_3}	mg/m^3	800-6200
pH	dimensionless	1-7
T	K	298±3

ond to ensure adequate image resolution. For each experimental condition, more than 400 drops were counted from photographs, then the diameter of each droplet was measured by image-processing software. In this paper, the Sauter mean diameter (SMD) was adopted to represent the mean droplet diameter [25]. To ensure measurement accuracy, a contrast experiment was conducted to measure the diameter of a falling plastic beads in practical diameter of 2 mm with the method just mentioned, and relative deviation of the real size and measured diameter was less than 5%.

THEORETICAL BASIS

1. Assumptions

The hydrodynamic and mass-transfer characteristics in spray tower are considerably complicated [26]. Specifically, the droplet size depends largely on both the nozzle structure and the spraying mechanism [27]. To find a simple approach for process simulation, a mathematical model has been developed based on the following assumptions:

1. Gas flow inside the absorber is considered to be plug flow. Neither collision, coalescence nor secondary breakup of the sprayed drops occurs in the absorption zone, and the drop size distribution can be represented by the mean droplet diameter. Furthermore, the drop is considered to be the rigid ball in shape and the vertical line in trace;

2. The reaction rates in liquid phase are much faster than the diffusion rates of both active components and dissolved ammonium species. Therefore, the chemical equilibrium, charge balance and ionic equilibrium in liquid phase are treated as instantaneous processes, and the resistance to diffusion is localized in a thin film adjacent to the gas-liquid interface;

3. The phase equilibrium prevails at the drop surface and gas dissolution obeys Henry's law. The effect of evaporation can be ignored, and the influence of mass transfer on the gas-liquid flow rates is negligible because the low NH_3 concentration.

2. Droplet Motion

First, we should find the hydrodynamic character in a spray tower. A well-known equation for particle motion is obtained by considering forces acting on a single droplet, as shown in Fig. 3.

$$\frac{\pi}{6}d^3\rho_1\frac{du_1}{dt}=\frac{\pi}{6}d^3(\rho_1-\rho_g)g-C_D\rho_g\frac{\pi}{4}d^2\frac{u_r^2}{2} \tag{1}$$

where $u_r=|u_l|+|u_g|$ is the droplet relative velocity; C_D represents the drag coefficient [28], which can be calculated by

$$C_D=\frac{24}{Re}(1+0.173Re^{0.657})+\frac{0.413}{1+16300Re^{-1.09}} \tag{2}$$

$Re=d\rho_g u_r/\mu_g$ is the Reynolds number of droplet. Currently, the buoyancy force can be ignored based on $\rho>>\rho_g$; thus, the differential equation of droplet motion is described as follows:

$$\frac{du_1}{dz}=\frac{g-A_J u_r^2}{u_1} \tag{3}$$

where, $A_J=3C_D\rho_g/4\rho_l d$, and the initial drop velocity is almost equal to the jet velocity u_0. Thus, the drop terminal velocity and the specific surface area along the absorption zone can be described by Eqs. (4) and (5), respectively.

$$u_T=\sqrt{\frac{g}{A_J}} \tag{4}$$

$$a=\frac{24L}{d\pi D_0^2 u_1} \tag{5}$$

3. Absorber Model

The reaction between NH_3 and HNO_3 can be considered as an instantaneous surface reaction. In such conditions, the liquid-phase mass transfer resistance might be neglected. Although such view has been accepted extensively [17,29], the practical mass transfer of NH_3 absorption into solution involves both gas- and liquid-side resistances. Based on the two-film theory, the mass transfer resistance concentrates on the gas- and liquid-film adjacent to the phase interface, as illustrated in Fig. 4.

For the infinitesimal layer of absorption zone, the mass balance of NH_3 is described by

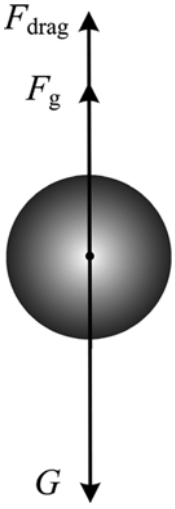

Fig. 3. Schematic diagram of forces acting on a droplet.

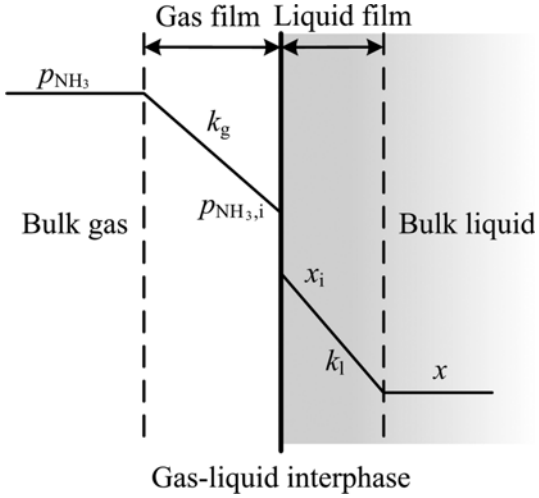

Fig. 4. Schematic diagram for NH_3 absorption into absorbent.

$$\frac{Q}{RT}dp_{NH_3}=\frac{\pi}{4RT}k_g a D_0^2(p_{NH_3}-p_{NH_3,i})dz=Ldx \quad (6)$$

where, p_{NH_3} and $p_{NH_3,i}$ are the partial pressure of NH_3 at the bulk gas and the interface, respectively; k_g is the gas-side mass transfer coefficient; x represents the total ammonium concentration in liquid phase. For the liquid-side mass transfer coefficient of NH_3, the expression used by Saboni has been adopted in this work [30]:

$$k_1=0.8\sqrt{\frac{D_1 u_T}{d}}\sqrt{\frac{C_D\rho_g}{2\rho_1}} \quad (7)$$

In the liquid phase, the active components can be completely consumed in a very short time according to the second assumption; thus, a reaction interface forms. When the concentration of active components in liquid phase increases, the reaction interface begins to move towards the phase interface; when the two interfaces coincide, the partial pressure of NH_3 at the interface is zero, and the liquid-phase mass transfer resistance vanishes.

Although several expressions of Sherwood number for gas-phase mass transfer coefficient (k_g) have been proposed in previous studies [26-28,31], we would like to develop a new approach for determining k_g. According to the Colburn analogy method:

$$\frac{Sh}{Re\cdot Sc^{1/3}}=\frac{f}{2} \quad (8)$$

where, $Sh=k_g d/D_g$, $Re=d\rho_g u_r/\mu_g$, $Sc=\mu_g/\rho_g D_g$. The droplet internal circulation velocity is much smaller than the relative dropping velocity between droplet and gas, so the surface velocity is approximately treated as zero. Moreover, the fanning friction factor (f) is only affected by the surface friction drag. Once the frictional drag is determined, the fanning factor can be obtained from Eq. (9):

$$F_\tau=\int_0^{2\pi}d\phi\int_0^{\pi}\left[\left(\frac{f}{2}\rho_g u_r^2\cdot\sin\theta\right)\cdot\left(\frac{d}{2}\right)^2\sin\theta\right]d\theta \quad (9)$$

Feng et al. obtained the numerical solution for the flow field distribution nearby the droplet surface [32]. The results indicate that the ratio of the frictional drag (F_t) and the total drag (F_{drag}) decreases with increasing the Reynolds number exponentially.

$$\frac{F_\tau}{F_{drag}}=6.8056Re^{-0.491} \quad (10)$$

$$F_{drag}=C_D\frac{\pi d^2}{4}\frac{\rho_g u_r^2}{2} \quad (11)$$

Thus, the fanning friction factor can be obtained according to Eqs. (9)-(11), and the Sherwood number can be developed and simplified as

$$Sh=1.083C_D Re^{0.509}Sc^{0.333} \quad (12)$$

The reasonability of Eq. (12) will be discussed later.

4. Ionic Equilibrium

When dilute NH_3 is absorbed into a droplet, the following reactions should be considered:

$$NH_3+H_2O=NH_3\cdot H_2O \quad H_{NH_3}=\frac{p_{NH_3}}{[NH_3]} \quad (13)$$

$$NH_3\cdot H_2O=NH_4^+ + OH^- \quad K_b=\frac{[NH_4^+][OH^-]}{[NH_3]} \quad (14)$$

$$H^+ + OH^- = H_2O \quad K_W=[H^+][OH^-] \quad (15)$$

Thus, the respective molarities of NH_3, and NH_4^+ in liquid phase are depended on the pH value. To determine the concentrations of NH_3 in the droplet, the following auxiliary variable is introduced:

$$x=[NH_3]+[NH_4^+]=[NH_3]\left(1+\frac{K_b}{K_W}[H^+]\right) \quad (16)$$

The major species in liquid phase are NH_3 NH_4^+ H^+ OH^- NO_3^-. In addition, $[NO_3^-]$ is constant for a certain initial component. The electroneutrality principle in liquid phase is expressed in the form

$$[H^+]+[NH_4^+]=[NO_3^-]+[OH^-] \quad (17)$$

If $[NH_4^+]$ and $[OH^-]$ are replaced by their combinations given by Eqs. (14) and (15), then Eq. (17) becomes Eq. (18):

$$\left(1+\frac{K_b[NH_3]}{K_W}\right)[H^+]^2-[NO_3^-][H^+]-K_W=0 \quad (18)$$

We can clearly see that Eq. (18) contains two opposite sign roots. Therefore, $[H^+]$ can be expressed as:

$$[H^+]=\frac{[NO_3^-]+\sqrt{[NO_3^-]+4K_W\left(1+\frac{K_b[NH_3]}{K_W}\right)}}{2\left(1+\frac{K_b[NH_3]}{K_W}\right)} \quad (19)$$

The observation of Eqs. (16) and (19) leads to the following relationship between concentration of dissociative ammonia and total ammonium in liquid phase.

$$x=[NH_3]\left(1+\frac{K_b[NO_3^-]+K_b\sqrt{[NO_3^-]^2+4K_W+4K_b[NH_3]}}{2K_W+2K_b[NH_3]}\right) \quad (20)$$

According to the two-film theory, the mass flux at the gas-liquid interface is given by

$$N=\frac{k_g}{RT}(p_{NH_3}-p_{NH_3,i})=k_1(x_i-x) \quad (21)$$

Moreover, according to Henry's law,

$$p_{NH_3,i}=H_{NH_3}[NH_3]_i \quad (22)$$

where, $[NH_3]_i$ represents the dissociative NH_3 concentration at the interface.

5. Parameters

On the basis of previous researches, the droplet diameter should be the most crucial one among the model parameters, which is determined by the liquid dispersion [12,33]. In this work, the mean droplet diameter is not a constant, which is primarily influenced by jet velocity, superficial gas velocity, physical properties of gas- and liquid-phase [23,25]. By fitting experimental data, an empirical correlation for mean droplet diameter can be expressed by Eq. (23):

$$d/d_0=2.04We^{0.11}Re_g^{-0.108} \quad (23)$$

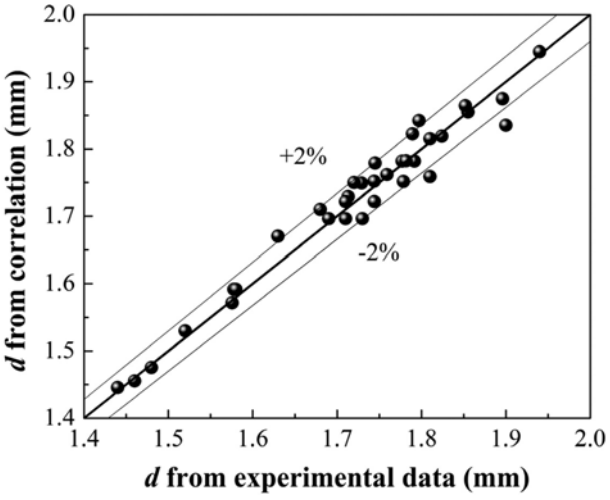

Fig. 5. A comparison between mean droplet diameter obtained from experimental data and correlation Eq. (23).

where, $We=d_0\rho_l u_0^2/\sigma_l$ represents the jet Weber number; $Re_g=D\rho_g u_g/\mu_g$ represents the gas Reynolds number. The effective ranges of Eq. (23) are as follows: $12\le We\le 115$, and $8{,}000\le Re_g\le 18{,}000$. The comparison (as shown in Fig. 5) reveals that the droplet diameter in our work can be described well by the correlation (Eq. (23)) with the maximum deviation about 2%. The formulas of remaining model parameters are summarized in Table 2 [18,31,34-37].

6. Calculation Process

The calculation procedure of the model is illustrated in Fig. 6. The calculation begins at the top of the absorber. The column is divided into n cells of height Δz, where the absorption rates are calculated by using the current concentrations in liquid bulk and partial pressures in gas bulk as the boundary conditions. In this paper n=100 is used to ensure enough precision. In every segment, the gas and liquid bulk concentrations are updated according to the transferred amount of different species. The dependent equations are composed of gas- and liquid-phase mass transfer coefficients, physical property parameters, etc. At present, the model is solved by the Newton iteration method, and the rigorously convergent criterion is presumed by requiring the relative difference between

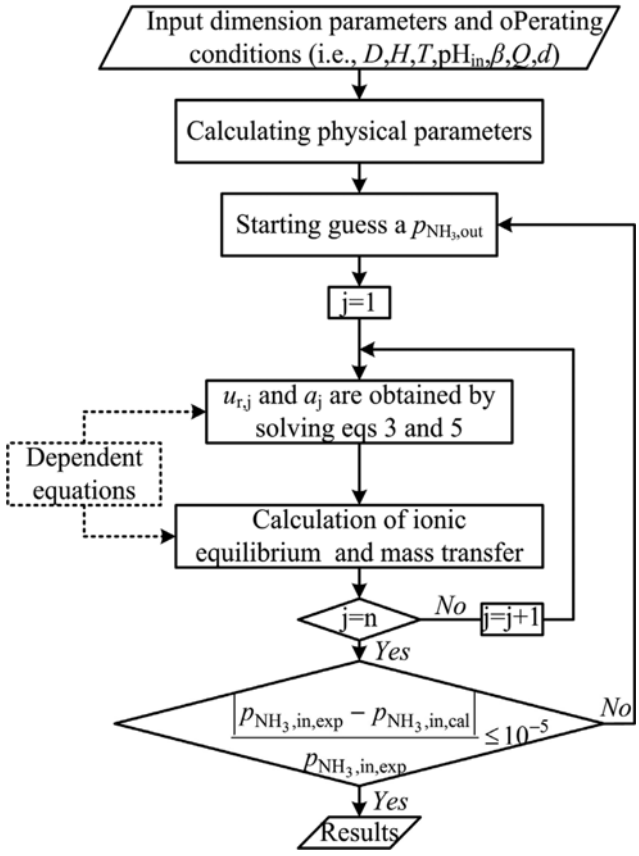

Fig. 6. The strategy of absorption efficiency estimation.

$p_{NH_3,in,exp}$ and $p_{NH_3,in,cal}$ is smaller than 10^{-5}. The observation of Fig. 6 shows that the program structure is quite concise. Thus, the simulate results can be conveniently obtained by taking a few seconds.

RESULTS AND DISCUSSION

The ambient temperature was about 298 K. Experiments on the NH_3 scrubbing have been conducted at various operating conditions as mentioned in Table 1. The percentage removal of NH_3 is calculated by the formula:

Table 2. Estimation of model parameters

Parameter	Unit	Formula	References
D_g	m^2/s	$9.86\times10^{-3}T^{1.75}p_{air}^{-1}\left[\frac{1}{M_{air}}+\frac{1}{M_{NH_3}}\right]^{0.5}\left(v_{air}^{1/3}+v_{NH_3}^{1/3}\right)^{-2}$	[31,36]
D_1	m^2/s	$\frac{2\times10^{-9}T\mu_1\vert_{298.15\,K}}{298.15\mu_1}$	[18,35]
H_{NH_3}	$Pa\cdot m^3/mol$	$\frac{10^5}{\rho_1}\exp\left(-\frac{7579.948}{T}-13.58857\ln T+0.008596972T+96.23184\right)$	[34]
K_b	mol/m^3	$\rho_1\exp\left(-\frac{5914.082}{T}-15.06399\ln T-0.01100801T+97.97152\right)$	[34]
K_W	mol^2/m^6	$\exp\left(14.01708-\frac{10294.84}{T}-0.0392282T\right)$	[37]

$$\eta = \frac{c_{NH_3,\,in} - c_{NH_3,\,out}}{c_{NH_3,\,in}} \times 100\% \quad (24)$$

An overall gas-phase mass transfer coefficient is defined by the following equation:

$$K_g = \frac{NRT}{p_{NH_3} - H_{NH_3}[NH_3]} \quad (25)$$

Thus, the fraction of gas-side mass transfer resistance can be described owing to Eq. (26):

$$K_g/k_g = \frac{NRT}{k_g(p_{NH_3} - H_{NH_3}[NH_3])} \quad (26)$$

1. Effect of Spray Density on Absorption Efficiency

The NH_3 absorption efficiency at pH=1 and pH=7 with a constant inlet NH_3 loading of 3,000 mg/m^3 has been plotted against spray density, as shown in Fig. 7. The absorption efficiency increases gradually with increasing the spray density, or decreasing the pH value. Such results are attributed to the interfacial contact area is in direct proportion to the spray density (Eq. (5)). Obviously, the simulation results agree well with the experimental data.

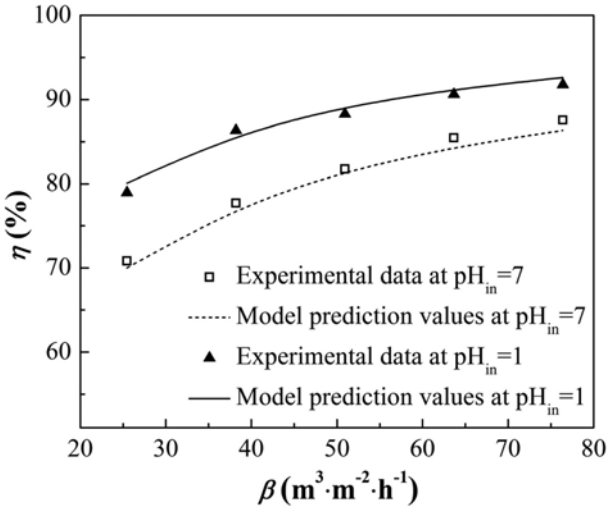

Fig. 7. Effect of spray density on absorption efficiency (u_g=1.95 m/s, $c_{NH_3,\,in}$=3,000 mg/m^3).

2. Effect of Superficial Gas Velocity on Absorption Efficiency

In Fig. 8, the absorption efficiency decreases linearly as the superficial gas velocity increases, and consistency is found between model and experimental results. Moreover, the absorption efficiency at pH=1 decreases slower than that of pH=7. Theoretically, the gas-side mass transfer coefficient can be enhanced slightly with the increase of superficial gas velocity [38]; meanwhile, the contact time between gas and droplets shortens [14], so absorption in the scrubber cannot proceed sufficiently. In addition, the consumption rates of active components in droplet rise, which further causes the decrease of absorption efficiency. This variation trend also supports the observation made by Turpin [29]. Besides, the absorptive capacity of absorbent increases with decreasing the pH value; thus, the evolution of absorption efficiency at pH=1 is relatively stable.

3. Effect of Inlet NH_3 Concentration on Absorption Efficiency

The variation of absorption efficiency with the inlet NH_3 loading is shown in Fig. 9. The experimentation reveals that the fluctuation of inlet NH_3 concentration in the range of 800-6,000 mg/m^3 has insignificant effect on the percentage removal. In fact, with increasing the inlet concentration of NH_3, the amount of removed NH_3 is increased, and both the numerator and the denominator of Eq. (24) are increased, almost to the same extent in the present case.

4. Effect of pH on Absorption Efficiency

Fig. 10 indicates that the percentage removal of NH_3 decreases initially with increasing the pH value and thereafter almost reaches a constant value when pH>3. Thus, the improvement of chemical reaction on the absorption efficiency is limited when pH>3. The reason can be explained as follows: with the decrease of pH value, the $[H^+]$ in the droplet is increased, hence the chemical reaction rate and absorptive capacity are both increased, and then the liquid-phase mass transfer resistance is weakened. The experimental

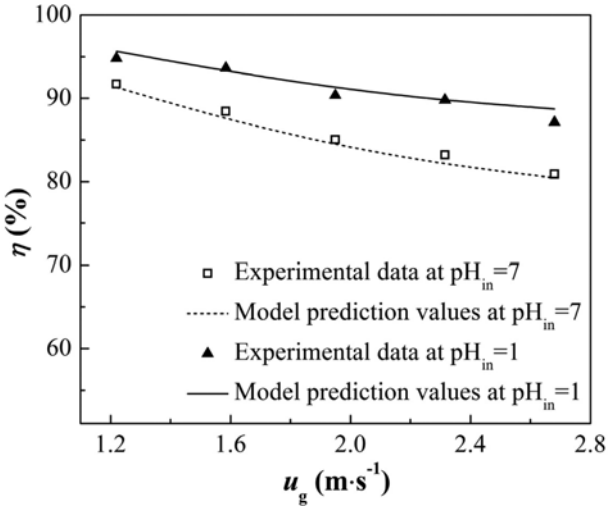

Fig. 8. Effect of superficial gas velocity on absorption efficiency (β=63.66 m^3/m^2·h, $c_{NH_3,\,in}$=3,000 mg/m^3).

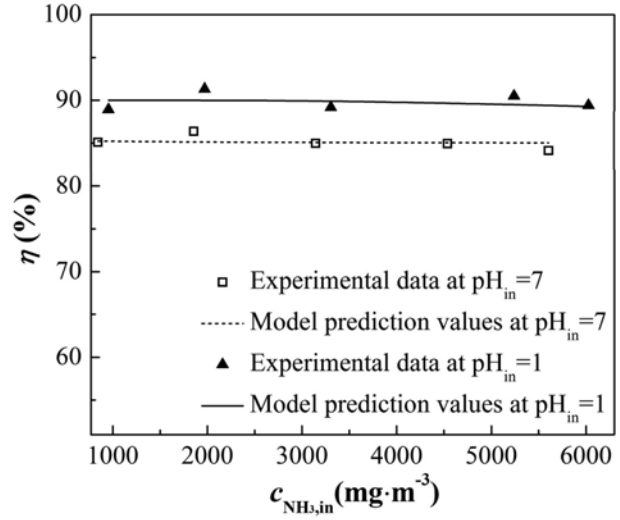

Fig. 9. Effect of inlet NH_3 concentration on absorption efficiency (β=63.66 m^3/m^2·h, u_g=1.95 m/s).

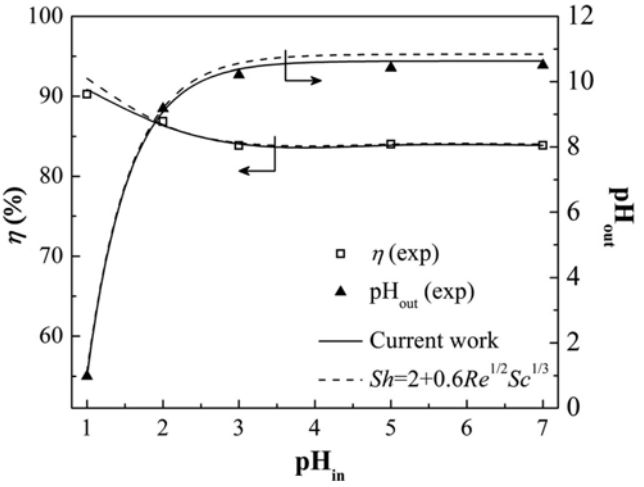

Fig. 10. Effect of pH value of absorbent on absorption efficiency (β=63.66 m^3/m^2·h, u_g=1.95 m/s, $c_{NH_3,in}$=3,000 mg/m^3).

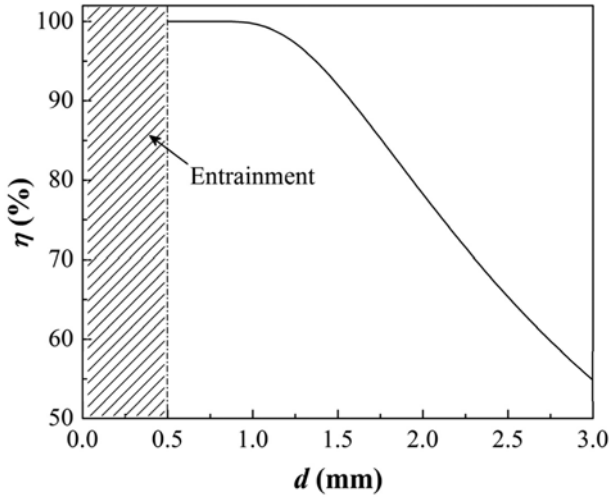

Fig. 11. Effect of mean droplet diameter on absorption efficiency (β=63.66 m^3/m^2·h, u_g=1.95 m/s, $c_{NH_3,in}$=3,000 mg/m^3, pH_{in}=7).

results also indicate that the pH value of 3 should be the obvious critical condition of transition between physical absorption and chemical absorption.

Several expressions of Sherwood number for gas-phase mass transfer coefficient have been proposed in previous studies. To attest that the derived formula for k_g in our work (Eq. (12)) is representative and applicative, the analogous simulation for predictions of both absorption efficiency and pH_{out} has been executed with different Sherwood numbers, and the classical Froessling correlation is cited [14,33].

$$Sh=2+0.6Re^{1/2}Sc^{1/3} \quad (27)$$

The observation of Fig. 10 shows that the values predicted by the present model are in good agreement with the experimental results, while predictions applied with the Froessling correlation, by contrast, have relatively low accuracy. It can be interpreted as the Froessling correlation (Eq. (27)) slightly overestimates the gas-side mass transfer coefficient and further enlarges the absorption rate.

5. Sensitivity Analysis

The model sensitivity to process parameters has been performed to evaluate its reliability [12]. A series of parameters have been identified to influence the model simulations based on the former researches [33,39], e.g., superficial gas velocity, spray density, liquid pH, inlet NH_3 concentration (see Table 3). Several representative parameter values have been designated in the analysis, and relative deviations of boundary values based on intermediate value of each item are equal to 50%. We can clearly see that the maximum deviation of absorption efficiency of each item varies between 6.9% and 14.6%. As the superficial gas velocity increases, the absorption efficiency decreases sharply; it approximately has the same but weaker influence of pH value on the efficiency. The spray density increase from 25 to 75 m^3/m^2·h has a positive effect on the efficiency ascribed to the more interfacial exchange area as well as the absorption capacity, and it can lead to an additional percentage removal of around 15.5%. As mentioned earlier, the inlet NH_3 loading has a negative but non-significant effect on the efficiency.

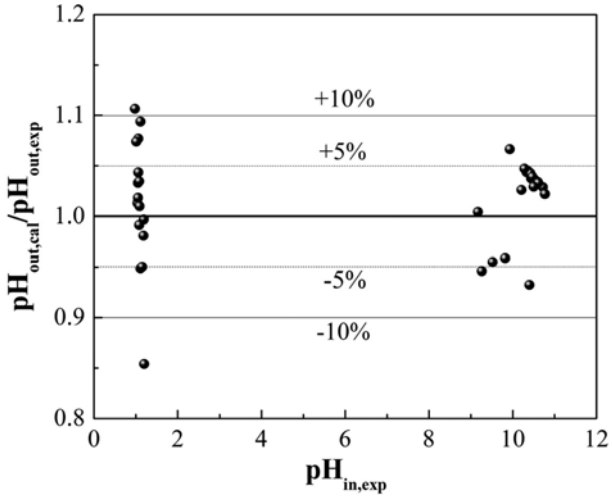

Fig. 12. Comparison of predicted values and experimental data for pH.

Another indeterminate parameter with intensive consideration is the mean droplet diameter (as shown in Fig. 11). Note that the variation of droplet diameter in the range of 1-3 mm has a signifi-

Table 3. Model sensitivity to process parameters

Parameter	Unit	Parameter value	Corresponding η (%)	Maximum deviation of η (%)
Superficial gas velocity	m/s	1, 2, 3	93.5, 84.0, 78.9	14.6
Spray density	m^3/m^2·h	25, 50, 75	80.0, 88.5, 92.4	12.4
Liquid pH	-	1, 2, 3	90.9, 86.4, 84.0	6.9

cant effect on the percentage removal. More specifically, the NH_3 removal efficiency increases from 78% to 100% with the decrease of droplet diameter from 2 to 1 mm. As the mean diameter decreases, both the mass transfer area and the contact duration between gas and liquid are augmented, which is similar to the given analysis results by Kallinikos, Neveux and Warych [12,27,33].

6. Distribution of Process Parameters along the Absorber

The outlet pH values of absorbent (pH_{out}) were measured in each experimental run. The comparison between predicted values and experimental data is shown in Fig. 12. The model results show a good agreement with the practical data. The maximum relative deviation is about 10%, and the majorities are less than 5%. Thus, the variations of pH value of drops can be well predicted by our model. Hence, the model enables us to predict the NH_3 capture process accurately.

Process simulation is a suitable way for assessing the absorber performance before performing tests on an industrial scale plant. As the droplets fall, absorption of NH_3 combined with chemical reactions gradually alkalizes the liquid. Generally, the pH value is minimum on top of the absorber but reversed at the bottom. These evolutions are presented in Fig. 13. Note that the variation of pH values along the tower is non-significant when pH_{in}=1. However, a sharp change occurs in liquid phase from acidity to alkalinity that can be detected when pH_{in} from 2 to 7. Besides, the pH curves with initial value of 5 and 7 are basically identical. Corresponding to pH_{in} of 2, 3, and 5, the dimensionless falling heights required for turning the basic droplet to the alkaline one are in the orders of 0.74, 0.12, and 0.01. Thereafter, the pH value of droplet tends to be stable, which implies that the capture process has been weakened.

The fraction of gas-phase mass transfer resistance (K_g/k_g) is an important parameter and a crucial reference for the interphase mass transfer [33,40]. Hence, a family of K_g/k_g curves can be obtained for different pH_{in}, as shown in Fig. 14. The result indicates that the mass transfer among this type of absorber, to a large extent, is gas-side mass-transfer-controlled. When pH_{in} ranges from 2 to 7, on the top of the absorber, K_g/k_g is high while the pH value is low (Fig. 13); then K_g/k_g decreases to about 75% at the bottom. By contrast, K_g/k_g for the NH_3 absorption system is about 80-90% in packed towers [17]. Particularly, when pH_{in}=1, the mass transfer resistance mainly lies on gas phase. Thus, as we continue to reduce pH_{in}, the absorption efficiency will remain unchanged, because the liquid-side mass transfer resistance is eliminated when pH_{in}<1. Note that the decrease of pH value does not always increase the absorption rate, but exacerbates the corrosion of equipment.

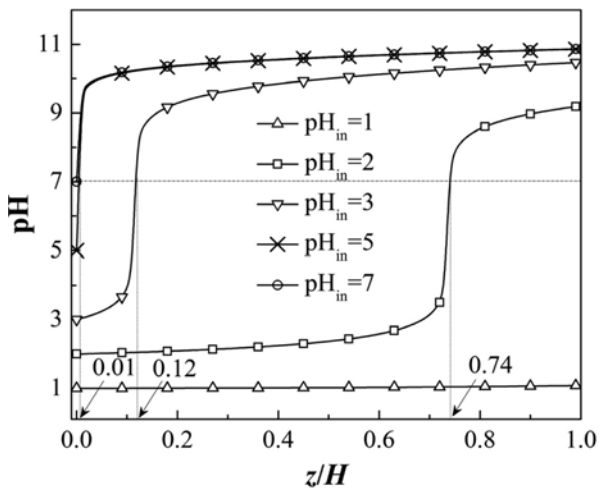

Fig. 13. The pH value of absorbent along the absorber.

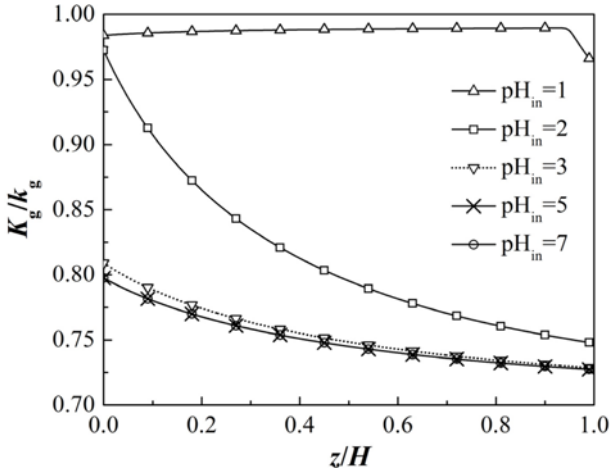

Fig. 14. The fraction of gas-phase mass transfer resistance profile.

CONCLUSIONS

An experimental study on ammonia absorption was conducted in a spray tower. A novel expression of Sherwood number for gas-phase mass transfer coefficient was presented based on the Colburn analogy method. A mathematical model for predicting the mass transfer performance in the absorber was developed based on both the two-film theory and the chemical equilibrium in liquid phase, and simulation results were in excellent agreement with experimental data. The results indicate that absorption efficiency increases with increasing spray density, and declines with increasing superficial gas velocity, pH value of absorbent and droplet diameter, and the inlet NH_3 concentration has insignificant effect on the percentage removal. The sensitivity analysis demonstrates that the mean droplet diameter should be the most crucial one among the model parameters, and an empirical correlation for the diameter is presented by fitting the experimental data. The initial pH value of absorbent has a significant effect on the fraction of gas-phase mass transfer resistance along the absorber, and the mass transfer resistance in liquid-side can only be neglected under certain ranges of acidity. Furthermore, our research results can provide some comprehensive guidance for both NH_3 capture in spray absorber and the theoretical constructions.

NOMENCLATURE

A_J : constant parameter [1/m]
a : specific surface area [m^2/m^3]
C_D : drag coefficient
c : NH_3 loading in gas phase [mg/m^3]
D : diffusion coefficient [m^2/s]

D_0 : inner diameter of spray tower [m]
d : mean diameter of droplets [m]
d_0 : orifice diameter of distributor [m]
F_{drag} : gas resistance [N]
F_g : buoyancy force [N]
F_τ : frictional drag force [N]
f : fanning factor
G : gravity [N]
g : gravitational acceleration [N/kg]
H : absorption height [m]
H_{NH_3} : Henry's coefficient of NH_3 for water [Pa·m^3/mol]
K_g : overall gas phase mass transfer coefficient [m/s]
K_b : dissociation equilibrium constant of $NH_3 \cdot H_2O$ [mol/m^3]
K_W : dissociation equilibrium constant of H_2O [mol^2/m^6]
k : mass transfer coefficient [m/s]
L : volumetric liquid flow rate [m^3/s]
M : molecular weight [g/mol]
N : mass flux [mol/m^2·s]
p : partial pressure of component [Pa]
Q : volumetric gas flow rate [m^3/s]
R : universal gas constant [J/mol·K]
Re : Reynolds number
Sh : Sherwood number
Sc : Schmidt number
We : Weber number
T : gas temperature [K]
t : time [s]
u : velocity [m/s]
u_0 : jet velocity [m/s]
[X] : concentration of X in liquid phase [mol/m^3]
x : total ammonium concentration in slurry [mol/m^3]
z : distance form distributor [m]

Greek Letters

β : spray density [m^3/m^2·h]
σ : surface tension coefficient [N/m]
η : absorption efficiency [%]
ρ : density [kg/m^3]
μ : viscosity [Pa·s]
ν : molecule volume [cm^3/mol]

Subscripts

cal : calculation
exp : experiment
g : gas
in : inlet of spray tower
i : interface
j : cell j
l : liquid or droplet
out : outlet of spray tower
r : relative
T : terminal

REFERENCES

1. C. H. Huang, *Environ. Eng. Sci.*, **22**, 535 (2005).
2. C. Pistarino, *J. Loss Prevent. Proc.*, **16**, 157 (2003).
3. A. P. Eremin, G. V. Kotov, T. V. Sidorovich and S. P. Fisenko, *J. Eng. Phys. Thermophys.*, **80**, 461 (2007).
4. S. K. Cho, M. K. Lee, D. H. Kim, Y. M. Yun, K. W. Jung, H. S. Shin and S. E. Oh, *Korean J. Chem. Eng.*, **31**, 619 (2014).
5. X. Guo, J. K. Tak and R. L. Johnson, *J. Hazard. Mater.*, **166**, 372 (2009).
6. T. Pröll, I. G. Siefert, A. Friedl and H. Hofbauer, *Ind. Eng. Chem. Res.*, **44**, 1576 (2005).
7. Y. Li, B. Sun, Z. Zeng, Y. Song, J. Chen, G. Chu, J. Chen and L. Shao, *Can. J. Chem. Eng.*, **93**, 116 (2015).
8. S. S. Kim, *Korean J. Chem. Eng.*, **32**, 303 (2015).
9. H. Jie, M. L. Jia, C. B. Tan and J. S. Sun, *Korean J. Chem. Eng.*, **28**, 2190 (2011).
10. Y. Lim, M. Choi, K. Han, M. Yi and J. Lee, *Ind. Eng. Chem. Res.*, **52**, 15131 (2013).
11. M. Ochowiak and L. Broniarz-Press, *Chem. Eng. Process.*, **50**, 345 (2011).
12. T. Neveux and Y. Le Moullec, *Ind. Eng. Chem. Res.*, **50**, 7579 (2011).
13. J. Zhu, S. C. Ye, J. Bai, Z. Y. Wu, Z. H. Liu and Y. F. Yang, *Fuel Process. Technol.*, **129**, 15 (2015).
14. Z. Shen, X. Chen, M. Tong, S. Guo, M. Ni and J. Lu, *Fuel*, **105**, 578 (2013).
15. M. Codolo, W. Bizzo and R. Bertazzoli, *Chem. Eng. Technol.*, **36**, 1255 (2013).
16. K. Ocfemia, Y. Zhang and Z. Tan, *Trans. ASAE*, **48**, 1561 (2005).
17. K. H. Javed, T. Mahmud and E. Purba, *Chem. Eng. Res. Des.*, **84**, 465 (2006).
18. L. Marocco, *Chem. Eng. J.*, **162**, 217 (2010).
19. M. C. Codolo and W. A. Bizzo, *Int. J. Heat Mass Transfer*, **66**, 80 (2013).
20. R. F. Adamowicz, *Atmos. Environ.*, **13**, 105 (1979).
21. I. Taniguchi, H. Yokoyama and K. Asano, *J. Chem. Eng. Jpn.*, **32**, 145 (1999).
22. Y. G. Adewuyi and G. R. Carmichael, *Atmos. Environ.*, **16**, 719 (1982).
23. F. V. Sirotkin and J. J. Yoh, *J. Comput. Phys.*, **231**, 1650 (2012).
24. N. Ashgriz, *Handbook of atomization and sprays: theory and applications*, Springer, New York (2011).
25. J. Zhu, Z. Y. Wu, S. C. Ye, Z. H. Liu, Y. F. Yang and J. Bai, *CIESC J.*, **65**, 4709 (2014).
26. L. Marocco and F. Inzoli, *Int. J. Multiphase Flow*, **35**, 185 (2009).
27. L. E. Kallinikos, E. I. Farsari, D. N. Spartinos and N. G. Papayannakos, *Fuel Process. Technol.*, **91**, 1794 (2010).
28. I. Tosun, *Modeling in transport phenomena: A conceptual approach*, Elsevier Science & Technology Books (2007).
29. A. Turpin, A. Couvert, A. Laplanche and A. Paillier, *Can. J. Chem. Eng.*, **87**, 53 (2009).
30. A. Saboni and S. Alexandrova, *Chem. Eng. J.*, **84**, 577 (2001).
31. Y. Zhong, X. Gao, W. Huo, Z. Y. Luo, M. J. Ni and K. F. Cen, *Fuel Process. Technol.*, **89**, 1025 (2008).
32. Z. G. Feng and E. E. Michaelides, *Int. J. Heat Mass Transfer*, **43**, 219 (2000).
33. J. Warych and M. Szymanowski, *Ind. Eng. Chem. Res.*, **40**, 2597 (2001).
34. K. Kawazuishi and J. M. Prausnitz, *Ind. Eng. Chem. Res.*, **26**, 1482

(1987).
35. W. H. Chen, *Atmos. Environ.*, **38**, 1107 (2004).
36. Y. Jia, Q. Zhong, X. Fan, Q. Chen and H. Sun, *Korean J. Chem. Eng.*, **28**, 1058 (2011).
37. V. Blanes-Vidal, S. G. Sommer and E. Nadimi, *Biosystems Engineering*, **104**, 510 (2009).
38. S. Ma, B. Zang, H. Song, G. Chen and J. Yang, *Int. J. Heat Mass Transfer*, **67**, 696 (2013).
39. T. Tanda, K. Shirai, Y. Matsumura and H. Kitahara, *Ind. Eng. Chem. Res.*, **50**, 13554 (2011).
40. B. Dou, W. Pan, Q. Jin, W. Wang and Y. Li, *Energy Convers. Manage.*, **50**, 2547 (2009).